Spatio-temporal filtering properties of a dendritic cable with active spines: a modeling study in the spike-diffuse-spike framework

Y Timofeeva* (yulia@ma.hw.ac.uk), G J Lord* (gabriel@ma.hw.ac.uk), and S Coombes† (stephen.coombes@nottingham.ac.uk)

Abstract

The spike-diffuse-spike (SDS) model describes a passive dendritic tree with active dendritic spines. Spine-head dynamics is modeled with a simple integrate-and-fire process, whilst communication between spines is mediated by the cable equation. In this paper we develop a computational framework that allows the study of multiple spiking events in a network of such spines embedded on a simple one-dimensional cable. In the first instance this system is shown to support saltatory waves with the same qualitative features as those observed in a model with Hodgkin-Huxley kinetics in the spine-head. Moreover, there is excellent agreement with the analytically calculated speed for a solitary saltatory pulse. Upon driving the system with time-varying external input we find that the distribution of spines can play a crucial role in determining spatio-temporal filtering properties. In particular, the SDS model in response to periodic pulse train shows a positive correlation between spine density and low-pass temporal filtering that is consistent with the experimental results of Rose and Fortune [1999, 'Mechanisms for generating temporal filters in the electrosensory system'. *The Journal of Experimental Biology* **202**, 1281–1289]. Further, we demonstrate the robustness of observed wave properties to natural sources of noise that arise both in the cable and the spine-head, and highlight the possibility of purely noise induced waves and coherent oscillations.

spike-diffuse-spike, dendritic spines, filtering, noise

1 Introduction

In 1891 Ramón y Cajal showed that dendritic spines are present in the dendrites of many neurons of the cerebral cortex of mammals [Cajal1891]. Dendritic spines are small mushroom like appendages with a bulbous head and

*Department of Mathematics, Heriot-Watt University, Edinburgh, EH14 4AS, UK.

†School of Mathematical Sciences, University of Nottingham, Nottingham, NG7 2RD, UK.

a tenuous stem (of length around 1μm) and may be found in their hundreds of thousands on the dendritic tree of a single cortical pyramidal cell. These extensions of the dendritic tree provide junction points for the axons of other neurons (i.e., provide surface area for synapses), and thus serve as loci for receiving inputs. In the cerebral cortex approximately 80% of all excitatory synapses are made onto dendritic spines. Since the biophysical properties of spines can be modified by experience in response to patterns of chemical and electrical activity, morphological and electro-chemical changes in populations of dendritic spines are thought to provide a basic mechanism for Hebbian learning in the nervous system. In fact as far back as 1899 Cajal (Cajal1899) was arguing that spines could be involved in learning and that physical changes in spines were associated with neuronal function, suggesting that they might grow with activity and retract during inactivity or sleep. These notions continue to be influential in the study of the function of dendritic spines even today [Yuste and Bonhoeffer2001, Yuste and Majewska2001].

In recent years the properties of spines have also been linked with the implementation of logical computations [Shepherd and Brayton1987] coincidence detection [Larkum et al.1999] orientation tuning in complex cells of visual cortex [Mel et al.1998] and the amplification of distal synaptic inputs [Miller et al.1985]. At the organismal level there is now evidence to suggest that the density of dendritic spines may reflect overall mental agility [Zito and Murthy2002]. Conversely, many neurological diseases resulting in mental retardation have been associated with spine loss or spine morphology changes (such as Fragile X-syndrome[1]). However, the focus of this paper will be on the implication of excitable channels in the spine-head membrane for single neuron dynamics. The benefits of excitable membrane for the amplification of excitatory synaptic inputs was first discussed by Jack et al. (Jack75). If dendritic spines possess excitable membrane, the spread of current from one spine along the dendrites may bring adjacent spines to threshold for impulse generation, resulting in a saltatory propagating wave in the distal dendritic branches [Shepherd et al.1985]. However, it is only relatively recently that confocal and two-photon microscopy observations have confirmed the generation of action potentials in the dendrites (see [Segev and Rall1998] for a perspective).

The first step towards the development of a spiny dendritic tissue model that might be used to explore these issues can be attributed to Baer and Rinzel (Baer91) who considered a passive uniform unbranched dendritic tree coupled to a population of excitable dendritic spines. In this *continuum* model the active spine-head dynamics is modeled with Hodgkin-Huxley (HH) kinetics whilst the (distal) dendritic tissue is modeled with the cable equation. The spine-head is coupled to the cable via a spine stem resistance that delivers a current proportional to the number of spines at the con-

[1] http://www.fraxa.org/

tact point. There is no direct coupling between neighboring spines; voltage spread by diffusion along the cable is the only way for spines to interact. Although the numerical studies of Baer and Rinzel (Baer91) show traveling wave solutions, the underlying continuous nature of the model precludes the possibility that these waves are truly saltatory. The saltatory nature of a propagating wave in a spiny neuron may be directly attributed to the fact that active spines are physically separated. Although we can numerically simulate the nonlinear and nonuniform properties of biologically realistic dendritic trees with discrete and clustered distributions of spines, based around natural extensions of the Baer-Rinzel (BR) model, there is a lack of analytical tools for dealing with such systems. However, recent work by Coombes, Bressloff and Lord [Coombes and Bressloff2000, Coombes2001b, Lord and Coombes2002, Coombes and Bressloff2003] has shown that the active membrane dynamics of spines can be treated using an analytically tractable integrate-and-fire (IF) process. The resulting model has been termed the Spike-Diffuse-Spike (SDS) model since spine-head dynamics is an all-or-nothing action potential response, whilst the dendritic cable is modeled as a passive structure. Not only can saltatory wave propagation be naturally analyzed in the SDS framework, the model is computationally inexpensive and ideally suited for the study of neural response to complicated spatio-temporal patterns of synaptic input that typically occur in cortical neurons. It is precisely these points we choose to highlight in this paper.

In section 2 we review the SDS framework and extend previous work by showing how one may express solutions in terms of a Dyson-like series expansion. Moreover, we discuss the numerical implementation of analytical solutions to the SDS model that depend upon numerically determined firing events. For comparison with more conventional (numerical PDE) approaches we also develop an implementation of the SDS model within the NEURON simulation environment [Hines and Carnevale2003]. As a first illustration of the usefulness of the SDS model of spiny dendritic tissue we present a case study of saltatory propagating waves in a model with regularly spaced spines. Also in section 3 we treat wave propagation (and its failure) for more irregular distributions of spines and relevant parameters. After establishing the ability of the SDS model to accurately describe the sorts of saltatory waves one finds in the more biophysically detailed BR model, we turn next, in section 4, to the issue of the active dendritic tree as a nonlinear filter. In particular we use the SDS model to address the observation of Rose and Fortune (Rose99) that there is a positive correlation between spine density and low-pass temporal filtering. In section 5 we test the robustness of observed wave and filtering properties to natural sources of noise that arise both in the cable and the spine-head, and highlight the possibility of purely noise induced waves and coherent oscillations. Finally, in section 6, we look forward and describe some of the open problems in single neuron function that may be readily addressed with a further analysis

of SDS dynamics.

2 The spike-diffuse-spike model

We consider a uniform passive dendritic cable with a given distribution of spines along its length. A schematic diagram of the SDS model is shown in Figure 1. The dynamics of membrane voltage in the cable $V = V(x,t)$ is

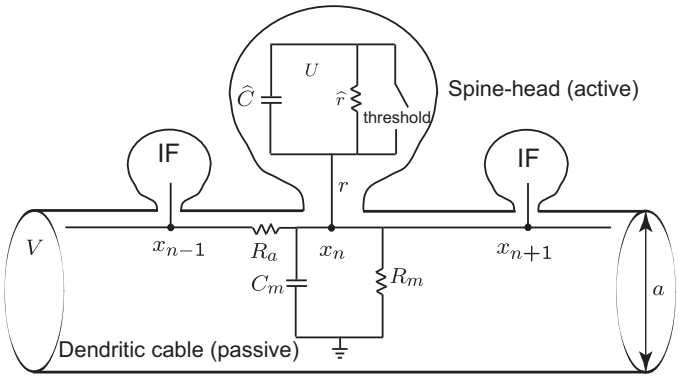

Figure 1: A schematic representation of the SDS model showing a passive cable with electrically connected active spines.

described by the equation

$$\pi a C_m \frac{\partial V}{\partial t} = \frac{\pi a^2}{4R_a}\frac{\partial^2 V}{\partial x^2} - \frac{\pi a}{R_m}V + \rho(x) I_{\rm sp}. \tag{1}$$

Here a is a diameter of the cable (measured in μm), R_a is the specific cytoplasmic resistivity (in Ω·cm), C_m and R_m are respectively the specific membrane capacity (in μF/cm^2) and a resistance across a unit area of passive membrane (in Ω·cm^2). Spines are connected to the cable at the discrete points x_n with the distribution function $\rho(x) = \sum_{n\in\Gamma}\delta(x - x_n)$, where Γ is a discrete set that indexes the spines. Each spine generates a sequence of action potentials in its spine-head given by the function $\widehat{V}(x,t)$. As a result the spine that just "fired" passes the spine current $I_{\rm sp} = (\widehat{V} - V)/r$ into the cable. The spine stem resistance of an individual spine is given by r. Denoting $T_n^m,\ m \in Z$ as the time of the mth firing event of the nth spine the function $\widehat{V}(x_n,t)$ is given by $\widehat{V}(x_n,t) = \sum_m \eta(t - T_n^m)$. Here $\eta(t)$ specifies the universal shape of an action potential. The generator of action potentials in the nth spine-head evolves according to

$$\widehat{C}\frac{\partial U_n}{\partial t} = -\frac{U_n}{\widehat{r}} + \frac{V_n - U_n}{r} - \underbrace{\widehat{C}h\sum_m \delta(t - T_n^m)}_{\rm reset}, \tag{2}$$

where $V_n = V(x_n, t)$. Here the parameters $\widehat{C}$ and $\widehat{r}$ describe the electrical properties of the spine-head membrane, namely its capacitance and resistance respectively. The spine's firing times T_n^m are defined in terms of the IF process according to

$$T_n^m = \inf\{t \mid U_n(t) \geq h,\ t > T_n^{m-1} + \tau_R\}. \tag{3}$$

Hence, a spine fires whenever U_n, driven by current from the shaft, crosses some threshold potential h. Just after the firing event the variable U_n resets to zero, modeled by the last term in equation (2). Multiple spiking events from an individual spine are controlled by a refractory time-scale τ_R during which the spine can not fire.

It is convenient to rewrite (1) in the standard form

$$\frac{\partial V}{\partial t} = D\frac{\partial^2 V}{\partial x^2} - \frac{V}{\tau} + Dr_a\rho(x)\frac{\widehat{V} - V}{r}, \tag{4}$$

where $D = \lambda^2/\tau$ denotes the diffusion coefficient of the cable, $\tau = C_m R_m$ is the membrane time constant, $\lambda = \sqrt{aR_m/4R_a}$ is the electronic space constant and $r_a = 4R_a/\pi a^2$ denotes the intracellular resistance per unit length of cable. The integration of this equation gives us an implicit expression for the membrane potential in the form

$$V(x,t) = \frac{Dr_a}{r}\sum_{k\in\Gamma}\int_0^t \mathrm{d}s\ G(x - x_k, t - s)[\widehat{V}(x_k, s) - V(x_k, s)]. \tag{5}$$

Here, $G(x,t)$ is the Green's function of the infinite uniform passive cable

$$G(x,t) = \frac{1}{\sqrt{4\pi Dt}}\ \mathrm{e}^{-\varepsilon t}\ \mathrm{e}^{-x^2/(4Dt)}\Theta(t), \tag{6}$$

where $\varepsilon = 1/\tau$ and $\Theta(t)$ is the Heaviside step function. The expression for the cable voltage (5) has a Dyson-like form [Bressloff and Coombes1997] suggesting a Neumann series solution, obtained by repeated substitution of (5) into itself. Introducing the parameter $\Lambda = Dr_a/r$, and generating just the first two terms in this expansion gives

$$\begin{aligned} V(x,t) &= \Lambda\sum_k \int_0^t \mathrm{d}s G(x - x_k, t - s)\widehat{V}(x_k, s) \\ &-\Lambda^2\sum_{k,p}\int_0^t \mathrm{d}s G(x - x_k, t - s)\int_0^s \mathrm{d}s' G(x_k - x_p, s - s')\widehat{V}(x_p, s'), \end{aligned} \tag{7}$$

where $\{p,k\} \in \Gamma$. Under the approximation that $\Lambda \ll 1$, only the first term in (7) significantly contributes to the full solution. This first term is an exact solution of the SDS model in the presence of a partial current $I_{\mathrm{sp}} = \widehat{V}/r$ from the spine-head into the cable instead of the original full current. This gives

rise to the so-called *partial SDS model*. For typical biophysically realistic parameter values Λ may vary between 0.01 and 0.3. This estimation is based on values of $D = 10^{-5}$ m^2/s, $r_a = 1.5 \times 10^9$ Ω/cm, and using the estimated range of $r = 5 - 150$ MΩ taken from the work of Svoboda et al. (Svoboda). Therefore, the partial model is a good approximation to the full model. In this case the solution takes the explicit form

$$V(x,t) = \Lambda \sum_{k\in\Gamma,m} H(x - x_k, t - T_k^m), \qquad \max_{k,m}\{T_k^m\} \le t < T_j^\ell, \tag{8}$$

where $m = m(k)$ counts firing events at each spine and $H(x,t) = \int_0^t G(x, t-s)\eta(s)\mathrm{d}s$. For a simple action potential shape given by a rectangular pulse $\eta(t) = \eta_0\Theta(t)\Theta(\tau_S - t)$ (with strength η_0 and duration τ_S), the function $H(x,t)$ can be found in closed form [Coombes and Bressloff2003] as $H(x,t) = A_\varepsilon(x, t - \min(t,\tau_S)) - A_\varepsilon(x,t)$ with a standard integral $A_\varepsilon(x,t)$ given in Appendix A. Equation (8) holds for times t between $\max_{k,m}\{T_k^m\}$ (i.e., the last firing event from the set of all spine firing times), and T_j^ℓ the time of the new firing event at the ℓth spine.

The firing times for the construction of solution (8) may be found from the set of threshold conditions $U_n(t) = h$, with $U_n(t)$ obtained by integrating equation (2). In particular, to find a new firing time $T_j^\ell > \max\{T_k^m\}$ corresponding to the spine at location x_j we have to solve the set of threshold conditions for the functions

$$U_n(t) = \frac{Dr_a}{\widehat{C}r^2} \sum_{k,m} \widehat{H}(x_n - x_k, t - T_k^m) - h \sum_m \mathrm{e}^{-\varepsilon_0(t - T_n^m)}, \tag{9}$$

where

$$\widehat{H}(x,t) = \int_0^t \mathrm{e}^{\varepsilon_0(s-t)} H(x,s)\mathrm{d}s, \tag{10}$$

and $\varepsilon_0 = (1/\widehat{r} + 1/r)/\widehat{C}$. For $\varepsilon > \varepsilon_0$ this integral can be found in closed form as $\widehat{H}(x,t) = (A_\varepsilon(x,0)(\mathrm{e}^{-\varepsilon_0(t - \min(t,\tau_S))} - \mathrm{e}^{-\varepsilon_0 t}) + \widehat{A}(x, t - \min(t,\tau_S)) - \widehat{A}(x,t))/\varepsilon_0$ with

$$\widehat{A}(x,t) = \mathrm{e}^{-\varepsilon_0 t}\left[A_{\varepsilon-\varepsilon_0}(x,0) - A_\varepsilon(x,0) - A_{\varepsilon-\varepsilon_0}(x,t)\right] + A_\varepsilon(x,t). \tag{11}$$

Alternatively the integral in (10) can be readily evaluated numerically for the explicitly given function $H(x,t)$.

By solving the set of threshold conditions with $U_n(t)$ defined by (9) we obtain a vector of times showing when each spine is able to reach the threshold h. The smallest time from this vector, T_j^ℓ, that satisfies the refractory restriction $T_j^\ell - T_j^{\ell-1} > \tau_R$ defines a new spiking event at location x_j. The firing times of an individual spine have to be separated by at least τ_S, so the refractory time is restricted by $\tau_R \ge \tau_S$. As a result of finding the newly fired spine extra terms have to be added into both sums in (9). The same routine is then repeated to obtain subsequent firing events.

2.1 Numerical implementation of the SDS model

The analytical integration of the equations of motion to get the explicit equations (8) and (9) for the partial SDS model obviates the need for the numerical solution of a partial differential equation. In the computations below we have taken $\varepsilon > \varepsilon_0$ so that the explicit solution (10) and (11) can be used. Up to determining the firing times this gives us an analytic solution. The numerical scheme for the explicitly defined solution was implemented in MATLAB and the firing times (defined from the threshold conditions $U_n(t) = h$) were determined numerically using the root-finding routine `fzero`. For each time interval the number of equations used for finding the earliest threshold crossing event can be reduced by excluding the spines that are still in the refractory state. Once the latest firing event has been determined then $V(x,t)$ can be evaluated (in terms of a sum over all spines and all previous firing events). Since contributions from firing events in the distant past are exponentially decaying it is safe to truncate this sum over events, and further improve numerical efficiency, though we do not do so in this paper.

In the following section we compare and validate the results from the (quasi) analytic solution of (10) and (11) detailed above. We show convergence by solving the explicit equation (7) for $V(x,t)$ rather than (8) which requires the solution of the differential equation (2) for each spine. We also compare to the SDS model given as a system of differential equations implemented in NEURON [Hines and Carnevale2003]. We solve the partial model with current $I_{\rm sp} = \widehat{V}/r$ from the spine-head into the cable as well as the full SDS model (1) and (2). We also compare to the BR model with discrete spines, again implemented in NEURON. All code is available upon request to the authors.

3 Validation of models and saltatory wave propagation

We validate the different models and their numerical solution by comparing the propagation of a solitary saltatory wave. We start by noting that for the (quasi) analytic case a solitary wave can be determined from the solution of a nonlinear algebraic equation.

Assume that the spines are regularly distributed along the cable with spacing d, i.e., $x_n = nd$. The speed of a solitary wave propagating in such a system may be determined in a self-consistent manner (see Coombes03) by the implicit equation

$$h = \frac{\Lambda}{\widehat{C}r} \sum_{n=1}^{\infty} \widehat{H}(nd, n\Delta), \tag{12}$$

for the partial SDS model. Here Δ measures the time between successive threshold crossings at adjacent spine-heads and thus the speed is $v = d/\Delta$.

In Figure 2 we plot this speed (solid curve) as a function of distance between the spines. If the spines are separated beyond some critical value (to the right of limit point LP) the wave fails to propagate. From the analysis in [Coombes2001a] it is further possible to establish that the faster of the two branches is stable. On the same figure we plot the results obtained from direct numerical simulations. In all simulations the wave is initiated from an activated single spine at one end of the cable (and free boundary conditions are assumed). Crosses indicate the speed obtained by using the explicit solution of the SDS model given by equations (8) and (9). Stars demonstrate the speed found by solving the system of differential equations. There is excellent agreement between both approaches as well as with the speed found from equation (12). Circles in Figure 2 denote the results of the full SDS model. The spine current passed into the cable in the full model is relatively less than in the partial model when other parameters are fixed. This explains why the wave in the last model propagates faster with the LP for propagation failure shifted to the right. If the firing events in the model are defined by using the full form of the solution for $V(x,t)$ given by equation (5) the results will agree with the numerical solution of the full SDS model. To demonstrate this convergence of the explicit approach, we evaluate the speed of wave propagation using the explicit equation (7) for $V(x,t)$ rather than (8). Equation (7) includes a second order term in Λ and this term has to be evaluated numerically. In this case the functions $U_n(t)$ used for the determination of firing events are found by solving the differential equation (2) for each spine. The obtained speed of the wave is indicated by triangles in Figure 2. The inclusion of the second order term in the expansion for the full solution yields a slower wave speed (than with just the first order term). As more terms are included in the expansion the wave speed gets closer to the solution of the full model. The inner plot in this figure is a magnified view (for small lattice spacing), and demonstrates that the speed of the wave attains a maximum for small d. In Figure 3 we plot the speed of a solitary wave as a function of the spine stem resistance r. As expected the speed decreases with increasing r and the wave fails to propagate when r is larger than about $r = 11.5$. In physical units this corresponds to a value of spine stem resistance of roughly 230 MΩ for a fixed spine spacing d of 0.01λ. Typical values of λ around 200 μm correspond to a spine spacing of around 2 μm (consistent with real spine spacing).

3.1 Validation against the Baer-Rinzel model

The SDS model defined in terms of the IF process is a reduced version of the biophysically realistic model of Baer91 where the spine-head dynamics are modeled by HH kinetics. To compare these two models, we consider the BR model with a discrete distribution of spines rather than with the spines uniformly distributed along the cable (Baer91, Lord02). In this case the

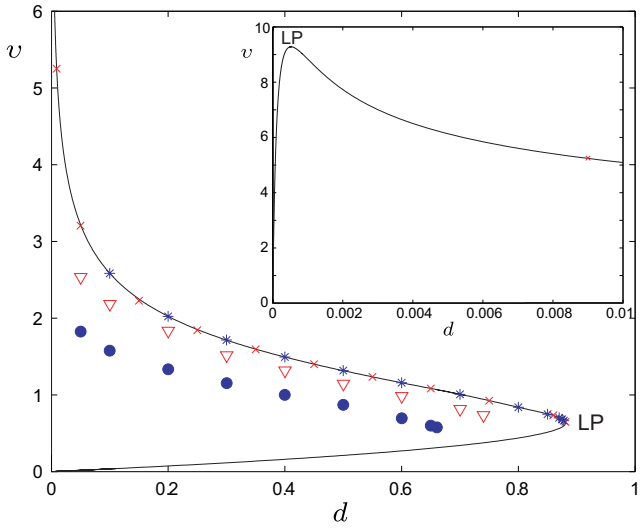

Figure 2: A plot of solitary wave speed v (in units λ/τ) as a function of the distance between the spines d (in units λ). Solid line: the solution of equation (12). Crosses: the solution given by the explicit equations (8) and (9). Stars and circles: the solutions defined by solving (1) and (2) for the partial and full SDS model respectively. Triangles: the solution defined by solving (2) and (7). Non-dimensionalized parameters: $D = 1$, $\tau_S = \varepsilon = 1$, $\eta_0 = 1$, $\varepsilon_0 = 0.8$, $\widehat{C} = 2.5$, $r = 1$ (corresponding to $r = 20$ MΩ in biophysical units), $\tau_R = 10$, $\widetilde{h} \equiv h/Dr_a = 0.05$. Inner plot is a magnified view of a part of the speed curve showing the LP for v.

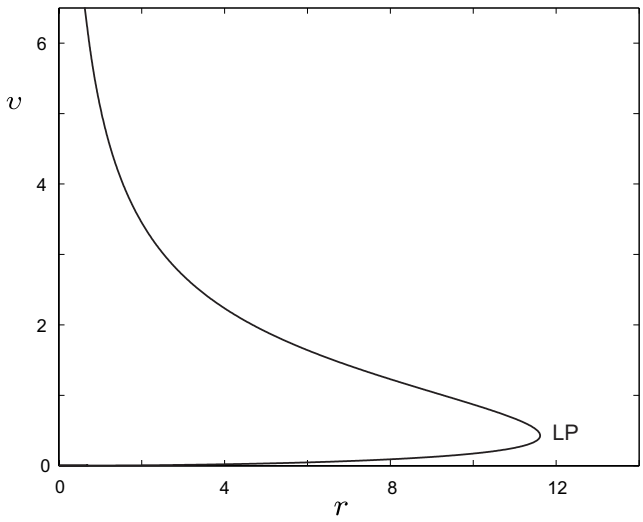

Figure 3: A plot of solitary wave speed v as a function of the spine stem resistance r when $d = 0.01$. Other parameters as in Figure 2.

model is defined by equation (1) and

$$\widehat{C}\frac{\partial \widehat{V}}{\partial t} = -I(\widehat{V}, m, n, h) - \frac{\widehat{V} - V}{r}. \tag{13}$$

Here the function I is the standard HH current, listed in Appendix B for completeness. The membrane current arises mainly through the conduction of sodium and potassium ions through voltage dependent channels in the membrane. A numerical simulation of the BR model with a regular distribution of spines is presented in Figure 4A which shows a space-time density plot of $V(x,t)$. This plot nicely illustrates an example of a saltatory traveling wave solution. Waves in the BR model travel in a saltatory manner because the discreteness of the spine distribution breaks the translation symmetry of the underlying cable. Although the wave has a saltatory nature it travels with a well-defined speed. This speed changes as we vary

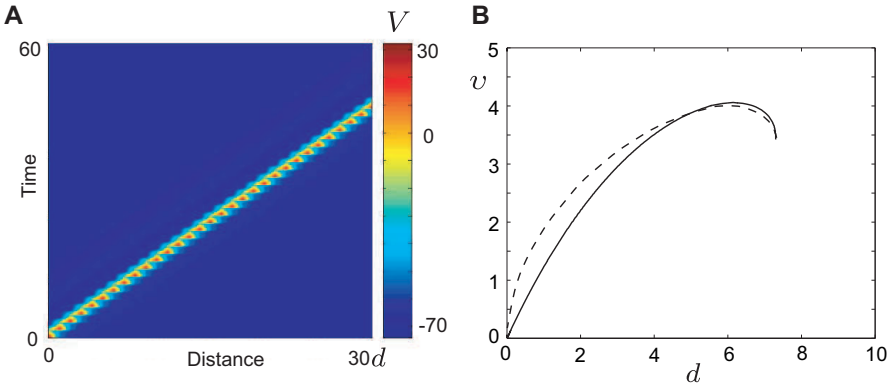

Figure 4: A: An example of saltatory traveling wave in the BR model with a discrete distribution of spines and spine spacing $d = 6$. B: The speed of wave propagation v as a function of the distance between the spines d in the discrete BR model (dashed curve) and in the partial SDS model (solid curve). Parameters of the SDS model: $D = 0.00012$ m^2/s, $\eta_0 = 100$ mV, $\tau_S = 2$ ms, $r = 4.5$ MΩ, $\widehat{C} = 0.0001$ μF, $\varepsilon = 3.35$, $\varepsilon_0 = 2.3$, $\tilde{h} \equiv h/r_a = 0.00095$. Other parameters for the BR model are given in Appendix B.

the distance between the spines, and is quantified in Figure 4B. Also in this figure we show a plot of the wave speed for the partial SDS model (solid curve), with parameters chosen so as to give a corresponding fit to the more biophysically detailed BR model.

From now on we consider the SDS model to be the (quasi) analytic solution of the partial SDS model obtained by solving equations (8) and (9) with a numerical approximation to the firing time.

3.2 Saltatory waves and spine distributions

As for the BR model with a discrete distribution of spines, the SDS model also supports saltatory traveling waves. For sufficiently small values of the refractory period it is possible to generate periodic traveling waves. In Figure 5A we show a space-time plot of the cable voltage V (in units of η_0) with 30 regularly distributed spines that nicely illustrates periodic wave propagation.

In real dendritic tissue the distribution of spines is likely to be irregular. In the SDS framework we might simply consider that the distribution function $\rho(x)$ has some disorder. An example of the effect that such disorder can have is shown in Figure 5B, where we choose spine positions from a uniform distribution. In comparison to Figure 5A, not only does this cause irregular wave propagation, but it may lead to back-propagating waves. As expected, too much spatial disorder in the spine distribution can lead to propagation failure, when any one pair of adjacent spines becomes too far separated to cause firing of one by the other. Moreover, in real dendrites there is heterogeneity not only in the distribution of spines, but in other system parameters, such as the refractory time scale and the spine stem resistance. In Figure 6 we show examples of wave propagation with a uniform distribution of refractory time scale over the spines (Figure 6A) and similarly for spine stem resistance (Figure 6B).

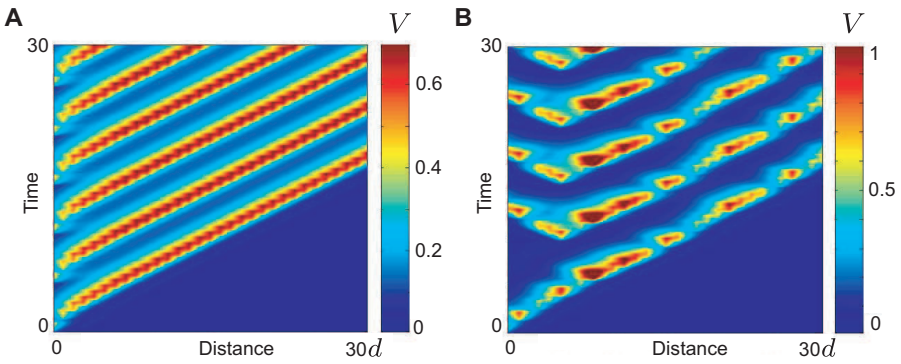

Figure 5: A: An example of a periodic traveling wave in the partial SDS model initiated from a single active spine and moving out through the cable with 30 regularly spaced spines when $d = 0.6$. Other parameters as in Figure 2 except $\tau_R = 5$. B: An example of irregular wave propagation in the partial SDS model for the parameter set corresponding to A (except $\tau_R = 6$) with 33 spine positions chosen from a uniform distribution (with mean 0.6 and variance 0.12).

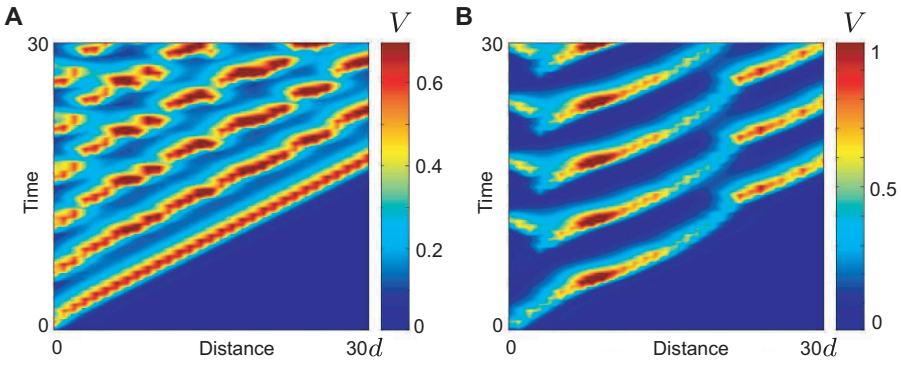

Figure 6: Examples of irregular wave propagation in the partial SDS model for the parameter set corresponding to Figure 5A with a uniform distribution of A: the refractory time τ_R (with mean 5 and variance 0.03) and B: the spine stem resistance r (with mean 1 and variance 0.08).

4 Filtering properties

The spatio-temporal patterns of activity in neurons and indeed networks of neurons is intimately linked to the processing of sensory information. A fundamental issue in understanding the relationship between structure and function is how neurons transform and represent information using such patterns. In this regard an understanding of how neural systems respond to sensory stimuli is an important issue. Indeed, although the selective behavioral responses to stimuli in the sensory systems of many organisms is believed to rely on the presence of filters for the neural representations of the temporal structure of sensory signals, the mechanisms underlying this temporal selectivity are not completely understood. Undoubtedly these mechanisms are subserved by the biophysics of neurons, including the passive electrical properties of a neuron, and the types and distribution of channels and conductances they support. However, only relatively recently has a role for dendritic spines begun to be seriously entertained. For an increased understanding of the role of spines in temporal filtering, intracellular recordings are necessary. Progress in recording from neurons as small as 10 μm has been made using 'patch-type' pipette techniques [Rose and Fortune1996], and these have been used to investigate the role of spines in filtering temporal input patterns to midbrain neurons of the weakly electric fish *Eigenmannia* [Fortune and Rose1997, Rose and Fortune1999]. In particular, this work has shown that neurons with a broad dendritic arbor and relatively spiny dendrites demonstrate low-pass temporal filtering properties in response to input stimuli. Here, we suggest the use of the SDS model for re-examining the findings of Rose and Fortune from a theoretical perspective, with a par-

ticular emphasis on clarifying the effect of both passive and active properties of the dendrite on filtering. The SDS model incorporates passive membrane properties within the cable and mimics active properties by the IF process in the spine-head. Importantly, we have the ability to vary spine distributions and see the effect on filtering. A limitation of the model is that no explicit consideration is given to the dynamics in the soma. However, output signal recordings at the soma in experiments are believed to be primarily influenced by the spread of activity in the dendrites, suggesting that an analysis of filtering within the SDS model will still be relevant.

We assume that an electrical signal in the form of a periodic pulse train is applied to the dendritic cable at position x_0. This is modeled by adding the following term to the right-hand side of equation (4)

$$I_{\text{stim}}(x,t) = \sum_p \delta(x - x_0)\delta(t - pT), \tag{14}$$

where T is the period of the stimulus. By solving equation (4) with this applied current, we obtain an extra term that enters the right hand side of equation (8) for the membrane potential as follows

$$\sum_{p=0}^{P} G(x - x_0, t - pT), \tag{15}$$

where $P = \max\{p \mid t - pT \geq 0\}$. Therefore, equation (9) for the spines has to be updated accordingly by adding an extra term

$$\frac{1}{r\widehat{C}} \sum_{p=0}^{P} \widehat{G}(x_n - x_0, t - pT), \tag{16}$$

where $\widehat{G}(x,t)$ is found as

$$\widehat{G}(x,t) = \int_0^t G(x,s)\mathrm{e}^{\varepsilon_0(s-t)}\mathrm{d}s = \mathrm{e}^{-\varepsilon_0 t}(A_{\varepsilon-\varepsilon_0}(x,0) - A_{\varepsilon-\varepsilon_0}(x,t)). \tag{17}$$

In Figure 7 we plot the results of simulations of the SDS model driven by the applied forcing signal (14). To study filtering properties we stimulated the system with a different fixed frequency. In all simulations the distribution of spines is chosen to be regular and the current is applied to the left end of the cable at a distance of 0.5 (in units of λ) from the first spine. Simulations show that differing applied stimuli lead to different patterns of wave propagation. The signal transformation during its propagation is best established by comparing the applied stimulus and the system response at the opposite end of the cable. If the period of stimulation is large, the signal measured at the end of the cable has a single inter-spike interval (ISI) consistent with the period of stimulus. If we decrease the period of stimulation

making it closer to the refractory time τ_R the output response at the end of the cable shows the presence of two ISIs. An example is shown in Figure 7. The plot on the right in this figure shows the membrane voltage at the location of the 55th spine along the cable. When the period of applied current is chosen to be small, the refractoriness of the system prevents the output from reaching the frequency of the stimulus. Instead, the system initiates repetitive waves consistent with the refractory time, with a single ISI.

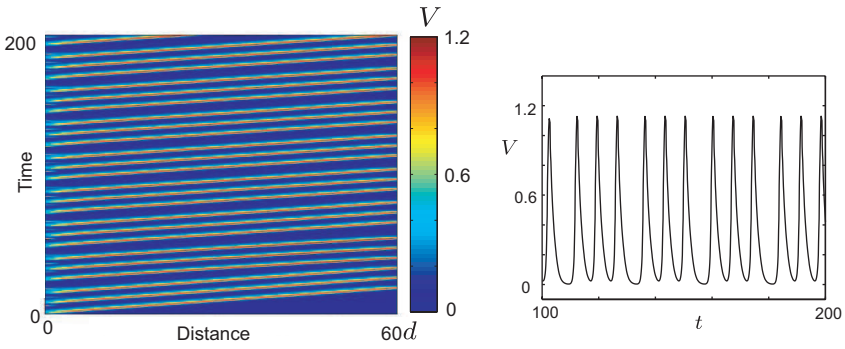

Figure 7: An example of wave propagation in the SDS model driven by periodic stimulation. The current stimulus is applied to the left end of the cable embedded with 60 regularly spaced spines. The system parameters as in Figure 2 with $d = 0.4$, except $\tau_R = 7$, and the period of stimulation $T = 6$. Plot on the right is an example of voltage profile at the location of the 55th spine along the cable.

The observed correlation between the periods of the applied signal and the ISIs of the system responses is quantified in Figure 8. The x-axis of the plots in this figure contains the frequencies of the applied stimulus used in the simulations. Along the y-axis we plot the frequencies at the end of the cable measured as the number of spikes emitted per unit time. Figure 8A shows the data from simulations for a spine spacing with $d = 0.4$. The vertical dashed line in this figure indicates the frequency of the applied signal of Figure 7. The two values for the spike frequencies that are defined for the particular range of input frequencies illustrate the presence of two distinct ISIs. The response of the system coincides with the input signal for low frequencies of stimulation, whereas for high frequencies it is limited by the system refractoriness. These dynamics indicate that the SDS model exhibits low-pass temporal filtering properties. The doubly periodic ISIs occur at stimulus periods close to the refractory time-scale. The smaller the distance between the spines, the smaller the range of input frequencies that lead to doubly periodic ISIs. However, if the spines are further apart, the regime of stimulus frequencies where the system responds irregularly with doubly periodic ISIs is increased. An example is shown in Figure 8B, where

the spine spacing d equals 0.8. Thus, the low-pass filtering properties are reduced with decreasing spine density.

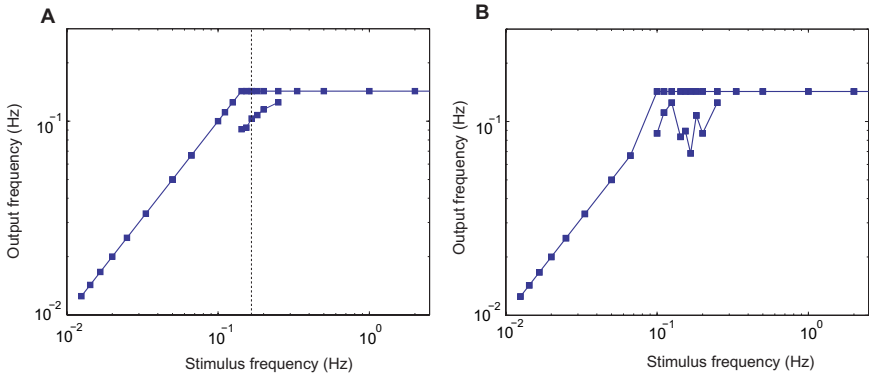

Figure 8: Frequency of the applied stimulation vs frequency of spikes in the output response at the end of the cable. The system parameters as in Figure 7 with $d = 0.4$ in A and $d = 0.8$ in B. Vertical dashed line in A indicates the frequency of stimulation that was chosen for simulations in Figure 7.

In Figure 9 we show the relative amplitude of voltage responses to the frequency of input current. This figure is included to make a link to the experimental observations that spiny neurons demonstrate a decline in the amplitude of voltage responses with increasing stimulation frequency. The relative amplitude measured in dB is evaluated as the difference between the maximum amplitude and the mean of the signal response. Figure 9A is plotted for two different spine spacings d. A decrease in the spine density (achieved by increasing d) reduces the decline in the voltage amplitude. The presence of doubly periodic ISIs in the voltage response causes the irregularities seen in both curves at periods around the refractory time-scale. In Figure 9B we show that a change in the refractory time in the system results in a shift of the original curve but does not affect the overall trend.

To summarize, the filtering properties of the SDS model are entirely consistent with the experimental observations of Rose and Fortune [Fortune and Rose1997, Rose and Fortune1999], namely that spiny dendrites with active membrane properties demonstrate low-pass temporal filtering properties.

5 Noise induced phenomenon

The spontaneous behavior of neurons *in vivo* is believed to be driven by voltage fluctuations arising from system noise. Such noise can be characterized as either intrinsic or extrinsic. A major source of intrinsic noise arises from the stochastic gating of ion channels in the cell membrane. Importantly, if

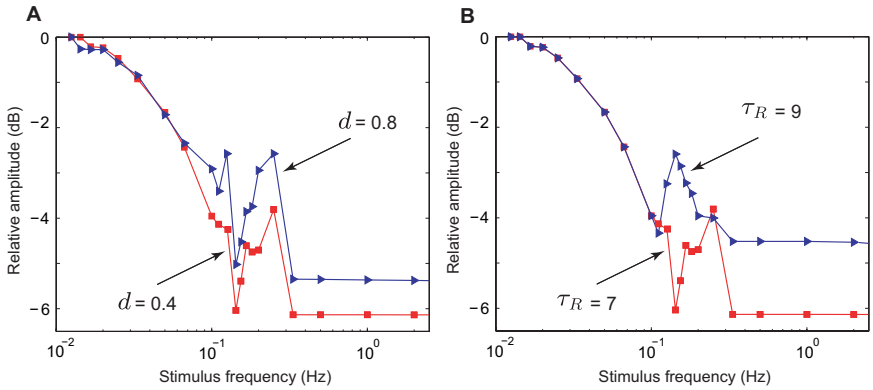

Figure 9: Frequency of applied stimulation vs relative amplitude of the voltage potential (in dB) with the system parameters as in Figure 7. A: $d = 0.4$ (squares), $d = 0.8$ (triangles), $\tau_R = 7$. B: $\tau_R = 7$ (squares), $\tau_R = 9$ (triangles), $d = 0.4$.

the membrane potential is close to threshold, channel noise can be critical for the generation of action potentials. In the SDS model the description of noise due to stochastic channels is best introduced in the excitable spine-heads. However, since the kinetics of ion channels are not explicitly included in the model, the noise is simply considered to lead to the stochastic generation of action potentials. Extrinsic noise sources in the neuron typically arise from synaptic inputs. Interestingly, there is an observed difference between the spontaneous activity of neurons *in vivo* and the activity during intracellular stimulation *in vitro*. Introducing a voltage fluctuation in the cable membrane as well as in the spines is a natural way to mimic the presence of input noise in the SDS model of an isolated neuron.

To study the effects of both types of noise on the properties of wave propagation in the SDS framework we assume that the system is driven by additive white noise in time that is either smooth (correlated) or white (uncorrelated) in space. The SDS model that includes noise both in the cable and the spine-head is given by

$$\mathrm{d}V = \left[D\frac{\partial^2 V}{\partial x^2} - \frac{V}{\tau} + Dr_a\rho(x)\frac{\widehat{V}-V}{r}\right]\mathrm{d}t + \mu_V \mathrm{d}W_V(t,x), \qquad (18)$$

$$\mathrm{d}U_n = \left[\frac{V_n}{\widehat{C}r} - \varepsilon_0 U_n - h\sum_m \delta(t - T_n^m)\right]\mathrm{d}t + \mu_U \mathrm{d}W_U(t,x). \qquad (19)$$

This is in fact a system of integral equations where we interpret noise in the Itô sense. We assume that the Wiener processes $W_{V,U}$ are of the form

$$W(t,x) = \sum_{n\in Z} b_n\phi_n(x)\beta_n(t)\ ,$$

where the β_n are a mutually independent ordinary set of Brownian motions. To simulate the Wiener process we took ϕ_n to be the eigenfunctions of ∂_{xx} with periodic boundary conditions. To avoid boundary effects this is done on a domain of twice the length of our computational domain. The coefficients b_n determine the spatial correlation. For spatially correlated noise we take

$$\sum_{n\in Z} e^{2\alpha|n|}|b_n|^2 < \infty \ ,$$

and here, the parameter α determines the correlation length scale and the spatial smoothness. The Brownian increment was implemented in a standard manner as discussed for example in [Kloeden and Platen1992]. We formed $W(t,x)$ with a fixed value of α, truncated the series with 512 terms and then took an interior portion of the same length as the computational domain. Examples of such noise are considered for example in [Da Prato and Zabczyk1992, Shardlow2005, García-Ojalvo and Sancho1999, Lord and Rougemont2004]. The parameters μ_V and μ_U describe the strength of the noise in the cable and in the spine-head respectively.

The integration of equation (18) for the membrane potential leads to a solution for $V(x,t)$ that may be split into two terms. The first term, representing the deterministic component, may be computed using the exact solution given by equation (8), whereas the second term incorporating the noise has to be evaluated numerically. The integration of equation (19) for $U_n(t)$, similarly to the cable, generates two terms. In general, the first term has to be evaluated numerically and we use an explicit Euler-Maruyama method. The second term, that defines the noise in the spine-head, was generated in the same manner as for the cable and then sampled at the spine position. However, when $\mu_V = 0$, the model reduces to the case where only the spines are forced by noise and, thus, the solution for $V(x,t)$ is explicitly defined. In this limit, the numerical evaluation of the first term in the solution of equation (19) can be avoided. Instead, this term is found using the explicit equation (9).

Here we demonstrate the effect noise can have on the properties of wave propagation in the SDS model. We begin by exploring the SDS model with noise only in the spine-head and take $\mu_V = 0$. In all of the figures that follow the noise-path is the same and μ_U is the only parameter that varies. In all simulations the spines are regularly distributed along the cable. When $d = 0.6$ (left of LP in Figure 2) the system supports wave propagation in the absence of noise. Further numerical simulations show that, in general, by increasing the level of noise in the system the patterns of cell response change from isolated or repetitive wave propagation to the case of almost simultaneous firing of all spines (i.e., a coherent behavior). However, at low noise levels the repetitive propagation of waves can be suppressed by a small noise increase. For high noise the majority of spines can generate an action potential immediately and this leads to the activation of residual

spines (i.e., those that did not fire) shortly thereafter. When $d = 1$ (right of LP in Figure 2) the system does not support traveling waves in the absence of noise. However, the examples in Figure 10 illustrate that noise can sustain spatio-temporal structures that could not otherwise occur. In particular, for a low level of noise we observe purely noise induced waves such as shown in Figure 10A. Propagation failure occurs if the level of noise is below some critical value. With high noise levels it is again possible to see coherent oscillations in the system (Figure 10B) where almost all spines simultaneously generate action potentials. Choosing uncorrelated white noise in the spine-head instead of correlated noise does not yield a qualitative change in system behavior.

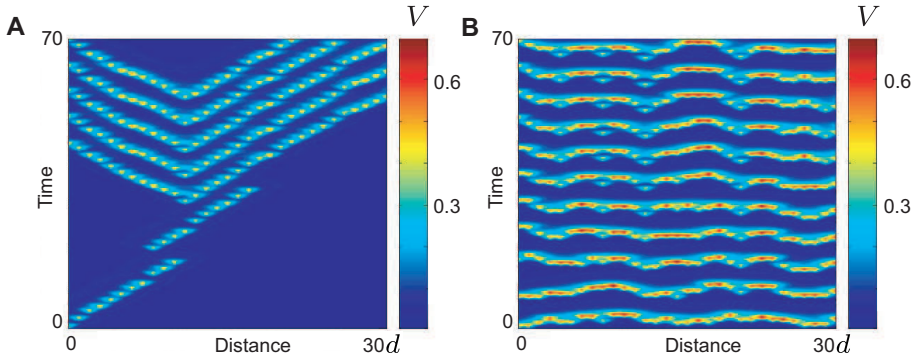

Figure 10: Traveling waves in the SDS model in the presence of correlated noise in the spine-heads for the parameters $\alpha = 1$, $d = 1$, $\mu_V = 0$ and A: $\mu_U = 0.17$, B: $\mu_U = 0.4$. Other parameters as in Figure 5A except $\tau_R = 6$.

The noise term in equation (19) for the spine-heads dynamics leads to a stochastic process for spike generation. Another way to incorporate this stochasticity into the firing events is to introduce a source of noise at the threshold level. This can be modeled under the replacement $h \to h+\xi$ where ξ is an additive noise with distribution $\rho(\xi)$. This approach can be simply implemented by generating a random vector ξ of length n from a distribution of mean h and standard deviation β at each small time step. Then the firing events are defined by checking the threshold conditions $U_n > \xi_n$ where ξ_n is the nth element of vector ξ and U_n is given by equation (9). The level of noise in the system is controlled by the parameter β. The numerical simulations of the SDS model in the presence of threshold noise demonstrate consistency with the results of the model driven by the stochastic forcing at the spine-heads. It is also possible to model the effect of threshold noise using a probabilistic rule for spike generation. To see this we consider drawing the threshold noise from a distribution σ, so that the probability of a firing event

can be written

$$P(U_n > h) = \int \sigma(\xi)\Theta(U_n - h - \xi)\mathrm{d}\xi = f(U_n - h), \tag{20}$$

where $f(\xi) = \int^{\xi} \sigma(x)\mathrm{d}x$. Considering a bell-shaped noise distribution for σ, then the function f will have a sigmoidal shape. Here we use the following form for the function f

$$f(U) = (1 + \mathrm{e}^{-\gamma h})/(1 + \mathrm{e}^{-\gamma U}) - \mathrm{e}^{-\gamma h}, \tag{21}$$

so that the probability of a firing event is zero and one respectively for $U = 0$ and $U \to \infty$. The parameter γ in (21) controls the level of noise in the system by determining the width of the bell-shaped distribution σ (such that decreasing γ corresponds to increasing noise). Simulation results of the SDS model with this probabilistic update rule are shown in Figure 11. Plots on the left are for the system with spine spacing $d = 0.6$, whereas plots on the right are obtained when $d = 1$. For low noise the system is able to support repetitive wave propagation as illustrated in Figures 11A and D. When the noise level is below some critical value, propagation failure occurs. This is similar to the behavior observed in our earlier examples of the stochastic SDS model. Here, however, an increase in noise causes more irregularity in the patterns of wave propagation (see Figures 11B and E). Moreover, high noise limits the spread of activity in the system by inhibiting wave propagation (see Figures 11C and F) or can even lead to propagation failure. The probabilistic rule used for the determination of the spikes in these last examples ensures that the firing probability of an individual spine is low if the membrane voltage in the cable at the location of this spine is low. This explains why wave propagation can terminate for high noise levels. In previous examples, where the noise in the spines is modeled by the stochastic differential equation (19), the high noise in the system, contrary to this last example, stimulates activity along the whole cable.

Now consider the stochastic SDS model driven by noise in the cable and thus, take $\mu_U = 0$. In the parameter region where waves propagate in the absence of noise ($d = 0.6$), an increase in noise level can lead to repetitive wave initiation. An example is shown in Figure 12 where we plot results of simulations for the system in the presence of correlated noise. The plot on the right shows the profile of an action potential in the membrane at the location of the 20th spine along the cable. In the presence of uncorrelated white rather than correlated noise, the system demonstrates a similar kind of behavior. If the distance between the spines is chosen to be large, the noise in the cable, correlated or white, is not able to initiate any wave propagation in the system. However, in the case of high white noise some limited activity was observed.

In summary, from our numerical simulations we conclude that noise in the spine-heads has a strong effect on the properties of wave propagation. In

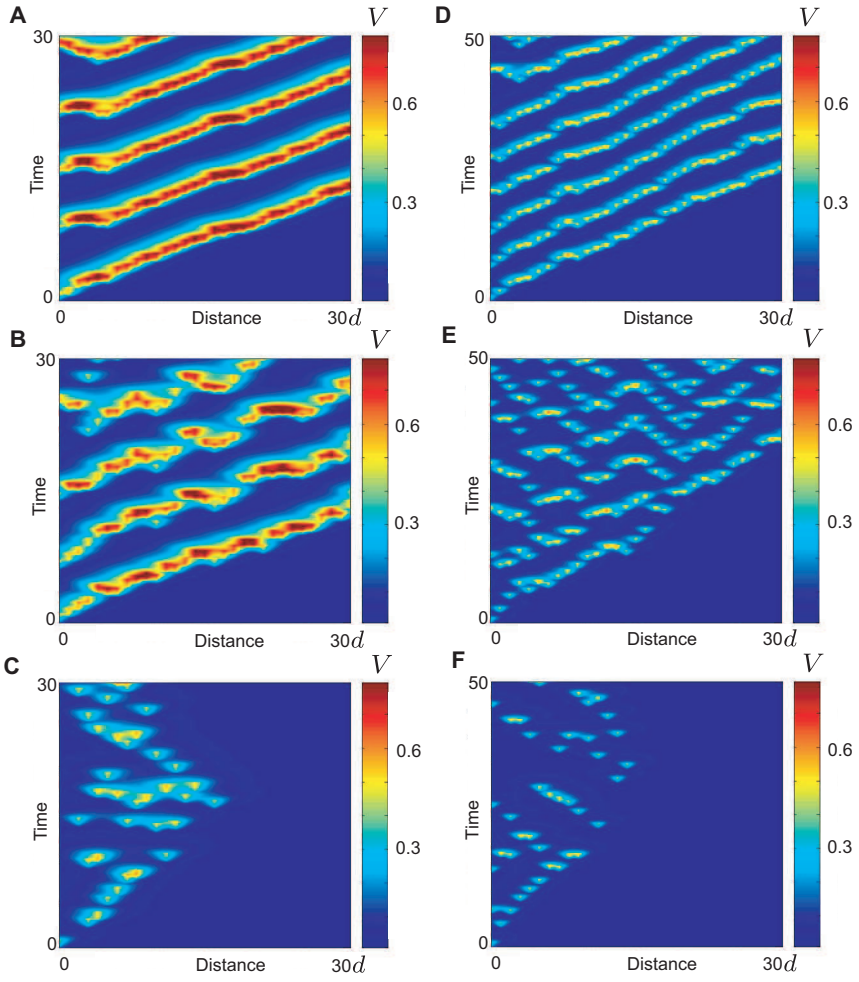

Figure 11: Traveling waves in the SDS model in the presence of threshold noise incorporated by the probabilistic rule for the spine spacing $d = 0.6$ (A, B and C) and $d = 1$ (D, E and F). The noise levels are $\gamma = 60$ (low noise) (A and D), $\gamma = 5$ (medium noise) (B and E), $\gamma = 0.8$ (C) and $\gamma = 1$ (high noise) (F). Other parameters as in Figure 5A except $\tau_R = 6$.

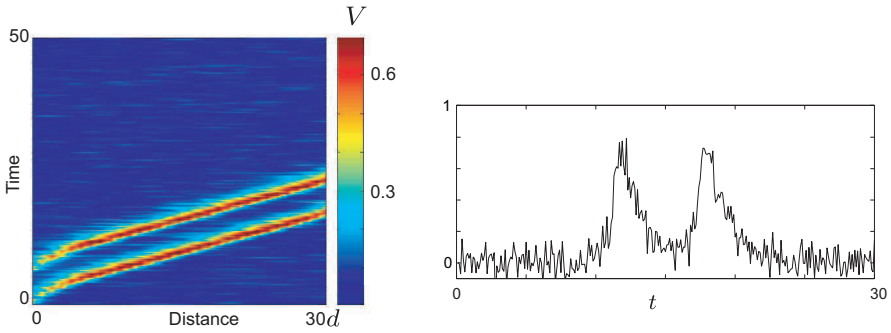

Figure 12: Traveling waves in the SDS model in the presence of correlated noise in the cable for the parameters $\alpha = 1$, $d = 0.6$, $\mu_U = 0$ and $\mu_V = 0.8$. Other parameters as in Figure 5A except $\tau_R = 6$. Plot on the right shows the profile of membrane voltage at the locations of 20th spine along the cable.

the parameter regime where the deterministic model fails to support waves, noise in the spines may aid in the initiation and propagation of waves. Moreover, for high noise in the spines one observes coherent oscillations. At the same time, the stochastic SDS model shows robustness of wave propagation to low noise in the spine-heads. On the other hand, noise in the cable does not have a strong effect on patterns of activity.

We now consider the presence of noise both in the cable and in the spine-heads (see Figure 13). Noise in the cable was chosen as for the model in Figure 12. Noise in the spine-heads is such that there is no repetitive firing without the added contribution from the cable. It is this combination that leads to more complex propagation patterns. Again we see in Figure 13B wave propagation in a regime where, with no noise, there is propagation failure.

Finally, we investigated the robustness of the filtering properties observed in the deterministic SDS model to noise sources. The SDS model in the presence of a small amount of correlated noise both in the cable and the spine-heads was driven by injected current in the form of a periodic pulse train as in section 4. Simulation results demonstrate that the presence of noise in the system yields qualitatively the same ISIs as in the deterministic model. Thus, in general the low-pass temporal filtering properties observed in the deterministic model are robust to noise.

6 Discussion

It is now just over one hundred years since the discovery of spines, yet there are still mysteries about the contribution they make to single neuron dynam-

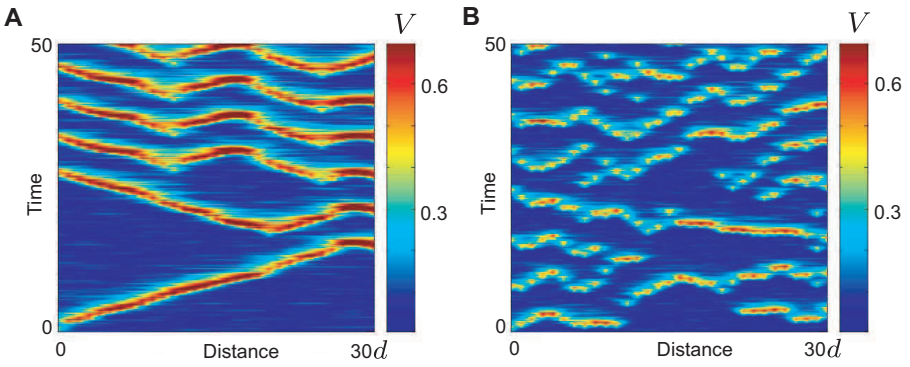

Figure 13: Traveling waves in the SDS model in the presence of correlated noise in the spines-heads and in the cable for the parameters A: $d = 0.6$, $\alpha = 1$, $\mu_V = 0.8$, $\mu_U = 0.07$ and B: $d = 1$, $\alpha = 1$, $\mu_V = 0.8$, $\mu_U = 0.2$. Other parameters as in Figure 5A except $\tau_R = 6$.

ics. Building on the insight into dendritic function gained since the pioneering theoretical work of Rall in the 1950's (surveyed in [Segev et al.1995]), we propose that the SDS model is ideally suited to probing how active spines shape and modulate a spatially structured input. In this paper we have focused on a rather simple (spatially localized) input, though we emphasize here that more spatially structured input can also be treated. Moreover, there is no barrier to working with a truly branched dendritic tree model as the analytical ("sum-over-paths") techniques necessary to do this have already been developed by Bressloff et al. (Bressloff96). Note that our study has concentrated on a typical value of spine stem resistance of 230 MΩ. However, spines which are both long and large can have higher resistances in the range 500-2000 MΩ [Benavides-Piccione et al.2002, Tsay and Yuste2004]. Hence, spine stem resistance is a bifurcation parameter worthy of future study, which we will consider elsewhere. In future work we propose to use the SDS model to understand whether inputs to a neuron sum linearly, or depend on spatial relationships in the input, such as clustering. The currently available experimental evidence is conflicting [Cash and Yuste1998, Polsky et al.2004]. Interestingly, recent advances in imaging technology (using fluorescent dyes in combination with confocal or two-photon laser scanning microscopy) have permitted time-lapse observation of spine morphology in living neurons [Fischer et al.1998, Dunaevsky et al.1999, Bonhoeffer and Yuste2002, Lippman and Dunaevsky2005, McKinney2005], showing that spines are also constantly moving. In fact over time-scales of seconds, spines continuously undergo small changes in shape, thought to be powered by dynamic actin filaments. On timescales of minutes to hours spines can change their shape dramatically or even appear or

disappear. Moreover, new spines can be generated in response to synaptic stimulation that also results in strengthening of synapses. These morphological changes could underlie some of the changes in synaptic strength induced by neural activity. Working within the SDS framework we would also be in a position to examine how successive synaptic input might influence spine motility and electro-chemical properties. Some work in this direction has already been done by Verzi et al. (Verzi05), for the continuum Baer and Rinzel model using phenomenological models of spine density dynamics. Within the SDS framework we envisage complementary work, building on existing modeling studies (of spines as calcium compartments) such as that of Holcman and Schuss (Holcman05), exploring how calcium accumulates in discrete spines, and how this makes its way to the cell nucleus and triggers genetic mechanisms that ultimately lead to the mechanical reconfiguration of the synapse. Both the above issues are topics of current investigation and will be reported upon elsewhere.

Acknowledgments

We would like to thank Steve Cox, Krešimir Josić and Costa Colbert for useful discussions about potential applications of the SDS model. The work in this paper is supported through EPSRC Grant No. GR/S60914/01. SC would also like to acknowledge ongoing support from the EPSRC through the award of an Advanced Research Fellowship, Grant No. GR/R76219.

Appendix A: $A_\varepsilon(x,t)$

$$\begin{aligned} A_\varepsilon(x,t) &= \frac{\eta_0}{4}\sqrt{\frac{1}{\varepsilon D}}\left\{\exp\left(-|x|\sqrt{\frac{\varepsilon}{D}}\right)\operatorname{erfc}\left(-\frac{|x|}{\sqrt{4Dt}}+\sqrt{\varepsilon t}\right)\right. \\ &+ \left.\exp\left(|x|\sqrt{\frac{\varepsilon}{D}}\right)\operatorname{erfc}\left(\frac{|x|}{\sqrt{4Dt}}+\sqrt{\varepsilon t}\right)\right\}. \end{aligned}$$

Appendix B: Equations of the BR model

$$\begin{aligned} I(\widehat{V},m,n,h) &= g_K n^4(\widehat{V}-v_K)+g_{Na}hm^3(\widehat{V}-V_{Na})+g_L(\widehat{V}-V_L), \\ \tau_X(\widehat{V})\frac{\mathrm{d}X}{\mathrm{d}t} &= X_\infty(\widehat{V})-X, \end{aligned}$$

for $X \in \{m,n,h\}$ where V_L, V_K and g_{Na} represent the constant membrane reversal potentials associated with the leakage, potassium and sodium chan-

nels respectively.

$$\tau_X(\widehat{V}) = \frac{1}{\alpha_X(\widehat{V}) + \beta_X(\widehat{V})},$$

$$X_\infty(\widehat{V}) = \alpha_X(\widehat{V})\tau_X(\widehat{V}),$$

where

$$\alpha_m(\widehat{V}) = \frac{0.1(\widehat{V}+40)}{1-\exp[-0.1(\widehat{V}+40)]},$$

$$\alpha_h(\widehat{V}) = 0.07\exp[-0.05(\widehat{V}+65)],$$

$$\alpha_n(\widehat{V}) = \frac{0.01(\widehat{V}+55)}{1-\exp[-0.1(\widehat{V}+55)]},$$

$$\beta_m(\widehat{V}) = 4.0\exp[-0.0556(\widehat{V}+65)],$$

$$\beta_h(\widehat{V}) = \frac{1}{1+\exp[-0.1(\widehat{V}+35)]},$$

$$\beta_n(\widehat{V}) = 0.125\exp[-0.0125(\widehat{V}+65)].$$

The following parameter values were used: $R_a = 100$ Ω·cm, $R_m = 3333$ Ω·cm^2, $C_m = 1$ μF/cm^2, $a = 0.5$ μm, $r = 5$ MΩ, $\widehat{C} = 0.0001$ μF, $g_L = 0.0003$ mS, $g_K = 0.036$ mS, $g_{Na} = 0.12$ mS, $V_L = -54.402$ mV, $V_K = -77$ mV and $V_{Na} = 50$ mV.

References

[Baer and Rinzel1991] Baer, S. M. and J. Rinzel: 1991, 'Propagation of dendritic spikes mediated by excitable spines: A continuum theory'. *Journal of Neurophysiology* **65**(4), 874–890.

[Benavides-Piccione et al.2002] Benavides-Piccione, R., I. Ballesteros-Yáñez, J. DeFelipe, and R. Yuste: 2002, 'Cortical area and species differences in dendritic spine morphology'. *Journal of Neurocytology* **31**(3-5), 337–346.

[Bonhoeffer and Yuste2002] Bonhoeffer, T. and R. Yuste: 2002, 'Spine motility: phenomenology, mechanisms and function'. *Neuron* **35**, 1019–1027.

[Bressloff and Coombes1997] Bressloff, P. C. and S. Coombes: 1997, 'Physics of the extended neuron'. *International Journal of Modern Physics B* **11**, 2343–2392.

[Bressloff et al.1996] Bressloff, P. C., V. M. Dwyer, and M. J. Kearney: 1996, 'Sum-over-paths approach to diffusion on trees'. *Journal of Physics A* **29**, 1881–1896.

[Cajal1891] Cajal, R.: 1891, 'Significación fisiológica de las expansiones protoplásmicas y nerviosas de la sustancia gris'. *Revista de ciencias medicas de Barcelona* **22**, 23.

[Cajal1899] Cajal, R.: 1899, 'Estudios sobre la cortexa cerebral humana: corteza visual'. *Rev. Trim. Microgr.* **4**, 1–63.

[Cash and Yuste1998] Cash, S. and R. Yuste: 1998, 'Input summation by cultured pyramidal neurons is linear and position independent'. *Journal of Neuroscience* **18**, 10–15.

[Coombes2001a] Coombes, S.: 2001a, 'The effect of ion pumps on the speed of travelling waves in the fire-diffuse-fire model of Ca^{2+} release'. *Bulletin of Mathematical Biology* **63**, 1–20.

[Coombes2001b] Coombes, S.: 2001b, 'From periodic travelling waves to travelling fronts in the spike-diffuse-spike model of dendritic waves'. *Mathematical Biosciences* **170**, 155–172.

[Coombes and Bressloff2000] Coombes, S. and P. C. Bressloff: 2000, 'Solitary waves in a model of dendritic cable with active spines'. *SIAM Journal on Applied Mathematics* **61**, 432–453.

[Coombes and Bressloff2003] Coombes, S. and P. C. Bressloff: 2003, 'Saltatory waves in the spike-diffuse-spike model of active dendritic spines'. *Physical Review Letters* **91**, 028102.

[Da Prato and Zabczyk1992] Da Prato, G. and J. Zabczyk: 1992, *Stochastic Equations in Infinite Dimensions*, Vol. 44 of *Encyclopedia of Mathematics and its Applications*. Cambridge University Press.

[Dunaevsky et al.1999] Dunaevsky, A., A. Tashiro, A. Majewska, C. Mason, and R. Yuste: 1999, 'Developmental regulation of spine motility in mammalian CNS'. *Proceedings of the National Academy of Sciences USA* **96**(23), 13438–13443.

[Fischer et al.1998] Fischer, M., S. Kaech, D. Knutti, and A. Matus: 1998, 'Rapid actin-based plasticity in dendritic spine'. *Neuron* **20**(5), 847–854.

[Fortune and Rose1997] Fortune, E. S. and G. J. Rose: 1997, 'Passive and active membrane properties contribute to the temporal filtering properties of midbrain neurons *In Vivo*'. *The Journal of Neuroscience* **17**, 3815–3825.

[García-Ojalvo and Sancho1999] García-Ojalvo, J. and J. M. Sancho: 1999, *Noise in Spatially Extended Systems*. Springer.

[Hines and Carnevale2003] Hines, M. L. and N. T. Carnevale: 2003, *The Handbook of Brain Theory and Neural Networks*, Chapt. The NEURON simulation environment, pp. 769–773. Cambridge, MA: MIT Press.

[Holcman and Schuss2005] Holcman, D. and Z. Schuss: 2005, 'Modeling calcium dynamics in dendritic spines'. *SIAM Journal on Applied Mathematics* **65**(3), 1006–1026.

[Jack et al.1975] Jack, J. J. B., D. Noble, and R. W. Tsien: 1975, *Electric Current Flow in Excitable Cells*. Clarendon Press.

[Kloeden and Platen1992] Kloeden, P. E. and E. Platen: 1992, *Numerical solution of stochastic differential equations*, Vol. 23 of *Applications of Mathematics*. Springer–Verlag.

[Larkum et al.1999] Larkum, M. E., J. J. Zhu, and B. Sakmann: 1999, 'A new cellular mechanism for coupling inputs arriving at different corticallayers'. *Nature* **398**, 338–341.

[Lippman and Dunaevsky2005] Lippman, J. and A. Dunaevsky: 2005, 'Dendritic spine morphogenesis and plasticity'. *Journal of Neurobiology* **64**(1), 47–57.

[Lord and Coombes2002] Lord, G. J. and S. Coombes: 2002, 'Traveling waves in the Baer and Rinzel model of spine studded dendritic tissue'. *Physica D* **161**, 1–20.

[Lord and Rougemont2004] Lord, G. J. and J. Rougemont: 2004, 'A numerical scheme for stochastic PDEs with Gevrey regularity'. *IMA Journal on Numerical Analysis* **24**, 587–604.

[McKinney2005] McKinney, R. A.: 2005, 'Physiological roles of spine motility: development, plasticity and disorders'. *Biochemical Society Transactions* **33**, 1299-1302.

[Mel et al.1998] Mel, B. W., D. L. Ruderman, and K. A. Archie: 1998, 'Translation-invariant orientation tuning in visual 'complex' cells could derive from intradendritic computations'. *The Journal of Neuroscience* **18**, 4325–4334.

[Miller et al.1985] Miller, J. P., W. Rall, and J. Rinzel: 1985, 'Synaptic amplification by active membrane in dendritic spines'. *Brain Research* **325**, 325–330.

[Polsky et al.2004] Polsky, A., B. W. Mel, and J. Schiller: 2004, 'Computational subunits in thin dendrites of pyramidal cells'. *Nature Neuroscience* **7**(6), 621–627.

[Rose and Fortune1996] Rose, G. J. and E. S. Fortune: 1996, 'New techniques for making whole-cell recordings from CNS neurons *In Vivo*'. *Neuroscience Research* **26**, 89–94.

[Rose and Fortune1999] Rose, G. J. and E. S. Fortune: 1999, 'Mechanisms for generating temporal filters in the electrosensory system'. *The Journal of Experimental Biology* **202**, 1281–1289.

[Segev and Rall1998] Segev, I. and W. Rall: 1998, 'Excitable dendrites and spines: earlier theoretical insights elucidate recent direct observations'. *Trends in Neuroscience* **21**(11), 453–460.

[Segev et al.1995] Segev, I., J. Rinzel, and G. M. Shepherd (eds.): 1995, *The theoretical foundations of dendritic function: selected papers of Wilfrid Rall with commentaries*. MIT Press.

[Shardlow2005] Shardlow, T.: 2005, 'Numerical simulation of stochastic PDEs for excitable media'. *Journal of Computational and Applied Mathematics* **175**(2), 429–446.

[Shepherd and Brayton1987] Shepherd, G. M. and R. K. Brayton: 1987, 'Logic operations are properties of computer-simulated interactions between excitable dendritic spines'. *Neuroscience* **21**(1), 151–165.

[Shepherd et al.1985] Shepherd, G. M., R. K. Brayton, J. P. Miller, I. Segev, J. Rinzel, and W. Rall: 1985, 'Signal enhancement in distal cortical dendrites by means of interactions between active dendritic spines'. *Proceedings of the National Academy of Sciences USA* **82**, 2192–2195.

[Svoboda et al.1996] Svoboda, K., D. W. Tank, and W. Denk: 1996, 'Direct measurement of coupling between dendritic spines and shafts'. *Science* **272**, 716–719.

[Tsay and Yuste2004] Tsay, D. and R. Yuste: 2004, 'On the electrical function of dendritic spines'. *Trends in Neurosciences* **27**(2), 77–83.

[Verzi et al.2005] Verzi, D. W., M. B. Rheuben, and S. M. Baer: 2005, 'Impact of time-dependent changes in spine density and spine shape on the input-output properties of a dendritic branch: A computational study'. *Journal of Neurophysiology* **93**, 2073–2089.

[Yuste and Bonhoeffer2001] Yuste, R. and T. Bonhoeffer: 2001, 'Morphological changes in dendritic spines associated with long-term synaptic plasticity'. *Annual Review of Neuroscience* **24**, 1071–1089.

[Yuste and Majewska2001] *Neuroscientist* **7**(5), 387–395.

[Zito and Murthy2002] Zito, K. and V. N. Murthy: 2002, 'Dendritic spines'. *Current Biology* **12**, R5.